Eur. Phys. J. B **32**, 329–338 (2003)
DOI: 10.1140/epjb/e2003-00106-7

THE EUROPEAN PHYSICAL JOURNAL B

Wigner lattice of ripplopolarons in a multielectron bubble in helium

J. Tempere[1,2], S.N. Klimin[1], I.F. Silvera[2], and J.T. Devreese[1,a]

[1] TFVS, Universiteit Antwerpen, Universiteitsplein 1, B2610 Antwerpen, Belgium
[2] Lyman Laboratory of Physics, Harvard University, Cambridge, Massachusetts 02138, USA

Received 20 February 2003
Published online 11 April 2003 –

Abstract. The properties of ripplonic polarons in a multielectron bubble in liquid helium are investigated on the basis of a path-integral variational method. We find that the two-dimensional electron gas can form deep dimples in the helium surface, or ripplopolarons, to solidify as a Wigner crystal. We derive the experimental conditions of temperature, pressure and number of electrons in the bubble for this phase to be realized. This predicted state is distinct from the usual Wigner lattice of electrons: it melts by dissociation of the ripplopolarons when the electrons shed their localizing dimple as the pressure on the multielectron bubble drops below a critical value.

PACS. 73.20.Qt Electron solids – 73.20.-r Electron states at surfaces and interfaces – 64.70.Dv Solid-liquid transitions – 68.35.Ja Surface and interface dynamics and vibrations – 47.55.Dz Drops and bubbles

1 Introduction

The two-dimensional (2D) electron system formed on the surface of liquid helium has been widely investigated, especially with regard to the formation and melting of a Wigner lattice [1]. An electric field pressing the electrons against the helium surface results in an interaction between the electrons and the quantized modes of oscillation of the helium surface, the ripplons [2]. In this paper, we investigate the effects of the electron-ripplon coupling in a multielectron bubble in liquid helium and highlight the differences with the case of electrons on a flat helium surface. Such multielectron bubbles (MEBs) are spherical cavities in liquid helium. MEBs are typically 0.1 μm–100 μm in radius for 10^3–10^8 electrons [3]. The bubble's diameter is determined by the balance between the surface tension of liquid helium and the Coulomb repulsion of the electrons [4].

The electrons are not distributed throughout the volume of the bubble, but form a nanometer thin and effectively 2D layer anchored to the inside of the bubble surface [5]. Although the flat 2D electron gas has been studied extensively and new quantum states such as the fractional quantum Hall regime were revealed, much less effort has gone to the study of the spherically curved 2D electron gas such as the one present in MEBs. Spherical shells of charged particles appear also in a variety of other physical systems, such as fullerenes [6], metallic nanoshells [7], and charged macroscopic droplets. The main goal of this paper is to show that the enhanced electron-ripplon coupling in the bubble leads to a new solid phase, a lattice of ripplonic polarons, that is distinct from the electron Wigner lattice, and to investigate the properties of this phase.

Using pressure, the surface of the MEB can be compressed to achieve 2D electron densities as high as 10^{14} cm^{-2} [8], whereas flat surfaces are limited to 2×10^9 cm^{-2} due to an instability [9]. This instability is not present in multielectron bubbles [10]. As a result very large electric fields exist on an electron, normal to the surface (due to all other electrons in the MEB), whereas for a flat surface the maximum field is around 3 kV/cm. Some typical values for physical variables related to the bubble are given in Table 1.

The Hamiltonian of a single electron on a flat helium surface is given by

$$\hat{H} = \frac{\hat{p}^2}{2m_e} + \sum_q \hbar\omega(q)\hat{a}^+_{\mathbf{q}}\hat{a}_{\mathbf{q}} + \sum_q M_q \mathrm{e}^{-\mathrm{i}\mathbf{q}.\mathbf{r}}\left(\hat{a}_{\mathbf{q}} + \hat{a}^+_{-\mathbf{q}}\right), \tag{1}$$

where $\hat{\mathbf{p}}$ is the electron momentum operator, m_e is the electron mass, and $\omega(q) = q\sqrt{\sigma q/\rho}$ is the ripplon dispersion relation with $\sigma \approx 3.6 \times 10^{-4}$ J/m^2 the surface tension of helium and $\rho = 145$ kg/m^3 the mass density of helium. In this Hamiltonian, we restrict ourselves to 2D position and momentum operators, assuming that the part of the wave function of the electrons relating to the direction perpendicular to the surface can be factored out exactly. The second-quantization operators $\hat{a}^+_{\mathbf{q}}, \hat{a}_{\mathbf{q}}$ create/annihilate a ripplon with planar wave number $\mathbf{q}$. The electron-ripplon

[a] *Also at:* TU Eindhoven, Eindhoven, The Netherlands
e-mail: devreese@uia.ua.ac.be

Table 1. For typical multielectron bubbles, the values of the several physical quantities are given at zero applied external pressure. The number of electrons in the bubble (N), the bubble radius (R_b), the average interelectron distance (d), the surface density of electrons (n_s), the pressing field generated by the electrons $|\mathbf{E}|$ (see Eq. (9)), the characteristic energy scale of the electron-ripplon interaction ($(e|\mathbf{E}|)^2/\sigma$, *cf.* formula (16)), and the characteristic frequency of the lattice potental (ω_{lat}) are given. Compare these quantities to, for example, the maximum density ($\approx 2\times10^9$ cm^{-2}) and the maximum pressing field (≈ 3 kV/cm) achievable on a flat helium surface over bulk.

N	$R_b(\mu\text{m})$	d(nm)	$n_s(\text{cm}^{-2})$
10^3	0.228	25.57	1.529×10^{11}
10^5	4.937	55.34	3.265×10^{10}
10^7	106.4	119.3	7.025×10^{9}
N	$\|\mathbf{E}\|$(kV/cm)	$e^2\|\mathbf{E}\|^2/\sigma$ (meV)	ω_{lat}(THz)
10^3	138.3	85.16	3.891
10^5	63.80	3.884	1.222
10^7	6.350	0.180	0.386

coupling amplitude is given by

$$M_q = \sqrt{\frac{\hbar q}{2\rho\omega(q)}}e|\mathbf{E}|, \tag{2}$$

where $\mathbf{E}$ is the electric field perpendicular to the surface (the so-called 'pressing field'), and e is the electron charge. The pressing field pushes the electrons with a force $e\mathbf{E}$ towards the helium surface, that acts like a sheet with surface tension σ. Note that there is a 1 eV barrier preventing single electrons from penetrating the helium surface. The self-induced trapping potential of the electron on the helium surface is manifested by the appearance of a dimple in the helium surface underneath the electron, much like the deformation of a rubber sheet when a person is pulled down on it by a gravitational force. The resulting quasiparticle consists of the electron together with its dimple and can be called a ripplonic polaron or ripplopolaron [11].

Hamiltonian (1) for the ripplopolarons is very similar to the Fröhlich Hamiltonian describing polarons [12]; the role of the phonons is now played by the ripplons. Methods suitable for the study of single polarons have been used to analyse the single ripplopolaron on a flat surface [13,14]. Recently, Fratini and Quémerais [15] have proposed a path integral treatment for a Wigner lattice of polarons. One of the goals of the present paper is to adapt their method so that it becomes suitable for the treatment of a lattice of ripplopolarons.

In Section 2 we introduce the Hamiltonian describing a ripplopolaron in a Wigner lattice of ripplopolarons in a multielectron bubble. The temperature zero solution for the ground state of this Hamiltonian is derived in the strong-coupling case in Section 3. The results for arbitrary interaction strength and arbitrary finite temperature, obtained with the variational path-integral technique, are presented in Section 4. These finite-temperature results allow us to investigate the melting of the ripplopolaron Wigner lattice and determine the phase diagram of this state in Section 5. The results are discussed and compared with the case of electrons on a flat helium surface in Section 6.

2 Hamiltonian for a ripplopolaron in a Wigner lattice

In their treatment of the electron Wigner lattice embedded in a polarizable medium such as a semiconductors or an ionic solid, Fratini and Quémerais [15] described the effect of the electrons on a particular electron through a mean-field lattice potential. The (classical) lattice potential V_{lat} is obtained by approximating all the electrons acting on one particular electron by a homogenous charge density in which a hole is punched out; this hole is centered in the lattice point of the particular electron under investigation and has a radius given by the lattice distance d. Thus, in their approach, the anisotropy effects are neglected. A second assumption implicit in this approach is that the effects of exchange are neglected. This can be justified by noting that for the electrons to form a Wigner lattice it is required that their wave function be localized to within a fraction of the lattice parameter as follows from the Lindemann criterion [16]. As can be read from Table 1, the typical distance between electrons (the lattice parameter) is 10–100 nm.

Within this particular mean-field approximation, the lattice potential can be calculated from classical electrostatics and we find that for a 2D electron gas it can be expressed in terms of the elliptic functions of first and second kind, $E(x)$ and $K(x)$,

$$V_{lat}(\mathbf{r}) = -\frac{2e^2}{\pi d^2}\left\{|d-r|\,E\left[-\frac{4rd}{(d-r)^2}\right] + (d+r)\,\mathrm{sgn}(d-r)\,K\left[-\frac{4rd}{(d-r)^2}\right]\right\}. \tag{3}$$

Here, $\mathbf{r}$ is the position vector measured from the lattice position. We can expand this potential around the origin to find the small-amplitude oscillation frequency of the electron lattice:

$$\lim_{r\ll d} V_{lat}(\mathbf{r}) = -\frac{2e^2}{d} + \frac{1}{2}m_e\omega_{lat}^2 r^2 + \mathcal{O}\left(r^4\right), \tag{4}$$

with the confinement frequency

$$\omega_{lat} = \sqrt{\frac{e^2}{m_e d^3}}. \tag{5}$$

Although this mean-field approach may seem crude, it has the distinct advantage that the 'phonon' frequency ω_{lat} of the electron lattice corresponds closely to the longitudinal plasmon frequency that can be derived using an entirely different approach based on a more rigorous study of the

modes of oscillations of both the bubble and the charge distribution on the bubble surface [17]. This frequency lies typically in the THz range and the lattice parameter d in MEBs ranges roughly from 10 to 100 nm. From this, and from the successful application of this mean-field approach to polaron crystals in solids, we conclude that the approach based on that of Fratini and Quémerais describes the influence of the other electrons well in the framework of small amplitude oscillations of the electrons around their lattice point. The (modified) Lindemann melting criterion suggests that the lattice will melt when the electrons are on average displaced more than ca. 10% from their lattice position; thus in the regime of interest the Fratini-Quémerais approach is applicable. In the mean-field approximation, the Hamiltonian for a ripplopolaron in a lattice on a *locally flat* helium surface is given by

$$\hat{H} = \frac{\hat{p}^2}{2m_e} + V_{lat}\left(\hat{\mathbf{r}}\right) + \sum_{\mathbf{q}} \hbar\omega(q)\hat{a}^+_{\mathbf{q}}\hat{a}_{\mathbf{q}} + \sum_{\mathbf{q}} M_q \mathrm{e}^{-\mathrm{i}\mathbf{q}\cdot\mathbf{r}}\left(\hat{a}_{\mathbf{q}} + \hat{a}^+_{-\mathbf{q}}\right), \tag{6}$$

where $\hat{\mathbf{r}}$ is the electron position operator.

Now that the lattice potential has been introduced, we can move on and include effects of the bubble geometry. If we restrict our treatment to the case of large bubbles (with $N > 10^5$ electrons) such as those already experimentally observed [3], then both the ripplopolaron radius and the inter-electron distance d are much smaller than the radius of the bubble R_b. This gives us ground to use the locally flat approximation using the auxiliary model of a ripplonic polaron in a planar system described by (6), but with a modified ripplon dispersion relation and an modified pressing field. In Appendix A we provide a more detailed description of the electron-ripplon interaction on a sphere and discuss how the locally flat approximation (6) is linked to the exact expressions for the curved surface. Essentially, we find for the modified ripplon dispersion relation in the MEB:

$$\omega(q) = \sqrt{\frac{\sigma}{\rho}q^3 + \frac{p}{\rho R_b}q}, \tag{7}$$

where R_b is the equilibrium bubble radius which depends on the pressure and the number of electrons [8]. The bubble radius is found by balancing the surface tension and the pressure with the Coulomb repulsion [8]. At zero pressure, it scales as $N^{2/3}$ and in the pressure-dominated regime ($p \gg \sigma/R_b$) it scales with pressure as $p^{-1/4}$. Some typical values are given in Table 1. The modified electron-ripplon interaction amplitude in an MEB is given by

$$M_{\mathbf{q}} = e|\mathbf{E}|\sqrt{\frac{\hbar q}{2\rho\omega(q)}}. \tag{8}$$

The effective electric pressing field pushing the electrons against the helium surface and determining the strength of the electron-ripplon interaction is

$$\mathbf{E} = -\frac{Ne}{2R_b^2}\mathbf{e}_{\mathbf{r}}. \tag{9}$$

Some typical values for the pressing field and the dimensionless coupling constants are given in Table 1. Note that the electric field in the bubble is larger than the typical pressing fields (of the order of $10^2 - 10^3$ V/cm) applied on electrons on a flat helium surface. Thus, the electron-ripplon coupling will be stronger in the multielectron bubble. The modified ripplon dispersion relation (and the dependence of the bubble radius on the number of electrons and the pressure) was studied in more detail in reference [8], and the stability of the multielectron bubble against surface deformational modes was investigated in detail in references [5,10]. These studies concluded that even though a large effective electric pressing field is present at zero pressure, the bubbles can be stable in contrast to the flat surface which can only sustain a moderate electric pressing field.

The crucial differences that exist between the case of a ripplopolaron in the multielectron bubble and on the flat surface (and that are preserved in the locally flat approximation) are (i) the electric pressing field $\mathbf{E}$ is stronger than that typically realized for electrons on helium films (see Tab. 1) and thus the electron-ripplon coupling is enhanced as compared to the normal film; (ii) the interaction energy arising from the change in polarisation of the helium due to the displacement of the electron has a similar form, but is much weaker and can be neglected. In addition the electric field, and thus the electron-ripplon coupling increases as the bubble radius is decreased. Thus, pressurizing the bubbles, which decreases the radius, also increases the electron-ripplon coupling strength (roughly as R_b^{-2}). In the high-pressure regime ($p \gg \sigma/R_b$), the bubble radius goes as $p^{-1/4}$ and thus the electron-ripplon coupling increases as $\sqrt{p}$. The pressure provides a 'tuning knob' to set the electron-ripplon interaction strength at a desired level.

3 The ripplopolaron Wigner lattice at temperature zero

3.1 Ground state

To gain insight into the nature of the Wigner solid of ripplopolarons, we will analyse Hamiltonian (6) first in the strong-coupling approach. In the next section, the more general and more accurate Feynman variational path-integral method will be applied, generalizing the results of this section to finite temperature. Noting that the frequency associated with the electron's motion, ω_{lat}, is typically several orders of magnitude larger than the frequency associated with the ripplons [17], $\omega(q)$, we can safely make the product ansatz for the wave function of the ripplopolaron in the lattice: $|\Psi\rangle = |\psi_e\rangle\,|\phi\rangle$. Here $|\phi\rangle$ is the factor of the wave function that contains the ripplon coordinates, and $|\psi_e\rangle$ is the electronic part of the wave function. For small-amplitude oscillations of the electrons around their lattice site, the lattice potential V_{lat} is well approximated by a parabolic potential (4), so we choose a Gaussian trial

wave function for the electronic part:

$$|\psi_e\rangle = \frac{1}{\pi^{1/2}a} \mathrm{e}^{-r^2/(2a^2)}. \tag{10}$$

In this trial wave function the variational parameter is a, the width of the electron wave function. Taking the expectation value of Hamiltonian (6) with respect to this electronic part of the wave function yields:

$$\langle\psi_e|\,\hat{H}\,|\psi_e\rangle = \frac{\hbar^2}{2m_e a^2} + \frac{m_e\omega_{lat}^2}{2}a^2 + \sum_{\mathbf{q}} \hbar\omega(q)\hat{a}_{\mathbf{q}}^+\hat{a}_{\mathbf{q}} + \sum_{\mathbf{q}} M_q \mathrm{e}^{-a^2q^2/4}\left(\hat{a}_{\mathbf{q}} + \hat{a}_{-\mathbf{q}}^+\right). \tag{11}$$

The ripplonic part of $\langle\psi_e|\,\hat{H}\,|\psi_e\rangle$ represents a displaced harmonic oscillator and can be rewritten as

$$\langle\psi_e|\,\hat{H}\,|\psi_e\rangle = \frac{\hbar^2}{2m_e a^2} + \frac{m_e\omega_{lat}^2}{2}a^2 - \sum_{\mathbf{q}} \frac{|M_q|^2\mathrm{e}^{-a^2q^2/2}}{\hbar\omega(q)} + \sum_{\mathbf{q}} \hbar\omega(q)\left[\hat{a}_{\mathbf{q}}^+ + \frac{M_q\mathrm{e}^{-a^2q^2/4}}{\hbar\omega(q)}\right]\left[\hat{a}_{\mathbf{q}} + \frac{M_q\mathrm{e}^{-a^2q^2/4}}{\hbar\omega(q)}\right]. \tag{12}$$

The ground state of the displaced (2D) harmonic oscillator at temperature zero has energy $\hbar\omega(q)$, independent of the variational parameter a. To find the variational optimal value of a, we minimize the ripplopolaron energy

$$E(a) = \frac{\hbar^2}{2m_e a^2} + \frac{m_e\omega_{lat}^2}{2}a^2 - \sum_{\mathbf{q}} \frac{|M_q|^2\mathrm{e}^{-a^2q^2/2}}{\hbar\omega(q)}\cdot \tag{13}$$

The sum over momenta can be rewritten as an integral, remembering

$$\sum_{\mathbf{q}} \to \int\limits_{q>1/R_b} \frac{\mathrm{d}^2\mathbf{q}}{(2\pi)^2} = \int\limits_{\tilde{q}>1} \frac{\mathrm{d}^2\tilde{\mathbf{q}}}{(2\pi)^2 R_b^2}\cdot \tag{14}$$

The lower limit appears since the largest wavelength available is $1/R_b$. We checked that the final results do not depend crucially on the value of this naturally occurring cut-off. A dimensionless integration variable $\tilde{\mathbf{q}} = \mathbf{q}R_b$ is introduced. The ground state energy of the ripplopolaron can then be evaluated analytically:

$$E(a) = \frac{\hbar^2}{2m_e a^2} + \frac{m_e\omega_{lat}^2}{2}a^2 - \frac{(e|\mathbf{E}|)^2}{2\pi\sigma}\int\limits_1^\infty \mathrm{d}\tilde{q}\frac{\tilde{q}}{\tilde{q}^2 + \frac{pR_b}{\sigma}}\exp\left[-\frac{a^2}{2R_b^2}\tilde{q}^2\right] \tag{15}$$

$$= \frac{\hbar^2}{2m_e a^2} + \frac{m_e\omega_{lat}^2}{2}a^2 - \frac{(e|\mathbf{E}|)^2}{4\pi\sigma}\exp\left[\frac{pa^2}{2\sigma R_b}\right]\Gamma\left[0, \frac{a^2}{2R_b^2}\left(1 + \frac{pR_b}{\sigma}\right)\right], \tag{16}$$

where Γ is the incomplete gamma function. Figure 1 shows the result for the variational parameter a as a function of number of electrons and pressure in the multielectron bubble. If this figure, a is expressed relative to the interelectron distance $\sqrt{4\pi R_b^2/N}$.

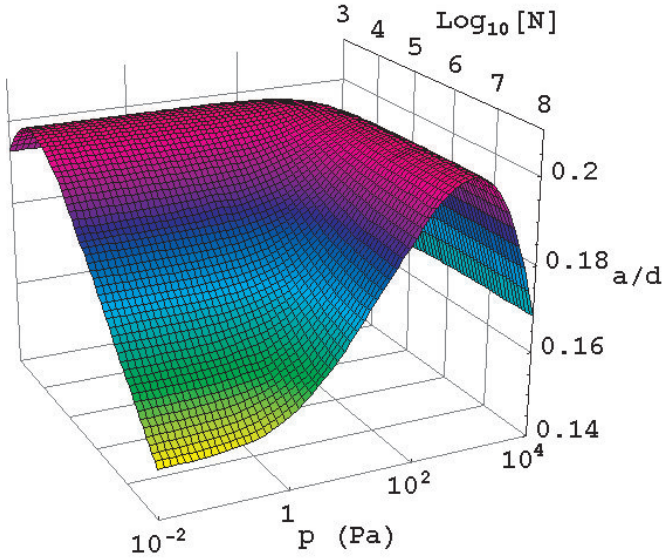

Fig. 1. The variational parameter a describing the width of the electron wave function in the strong-coupling approach as a function of number of electrons and pressure in the multielectron bubble. d is the interelectron separation.

3.2 Dimple shape

The ripplonic part of the Hamiltonian (12) represents oscillations of the helium surface no longer around the original bubble surface, but around a new, displaced equilibrium surface. This displacement of the helium surface is the dimpling. Underneath each electron, a dimple appears. The new equilibrium surface, described by the function $u(\mathbf{r})$ (*cf.* appendix, Eq. (39)), can be found by using the canonical relation between the surface displacement operator and the ripplon creation and annihilation operators:

$$\hat{Q}_{\mathbf{q}} = \sqrt{\frac{\hbar q}{2\rho\omega(q)}}(\hat{a}_{\mathbf{q}} + \hat{a}_{-\mathbf{q}}^+), \tag{17}$$

and evaluating

$$u(\mathbf{r}) = \sum_{\mathbf{q}} \langle\Psi|\,\hat{Q}_{\mathbf{q}}\,|\Psi\rangle\,\mathrm{e}^{\mathrm{i}\mathbf{q}\cdot\mathbf{r}}. \tag{18}$$

The result is given by

$$u(\mathbf{r}) = \frac{e|\mathbf{E}|}{2\pi\sigma}\int_1^\infty \mathrm{d}\tilde{q}\frac{\tilde{q}}{\tilde{q}^2 + \frac{pR_b}{\sigma}}J_0\left(\frac{\tilde{q}r}{R_b}\right)\mathrm{e}^{-a^2\tilde{q}^2/(4R_b^2)}. \tag{19}$$

In the limiting case of a large bubble, this result corresponds to that of Shikin and Monarkha [11] for electrons on a flat helium surface; the role of the capillary constant is played by $p/(\sigma R_b)$. Figure 2 shows, for a bubble with $N = 10^5$ electrons, at different pressures the shape of the dimpled surface. Several dimples are shown – above the center of each dimple an electron is present. The dotted curve represents the undimpled $u(\mathbf{r}) = 0$ surface; the curvature of the bubble surface is visible in this curve.

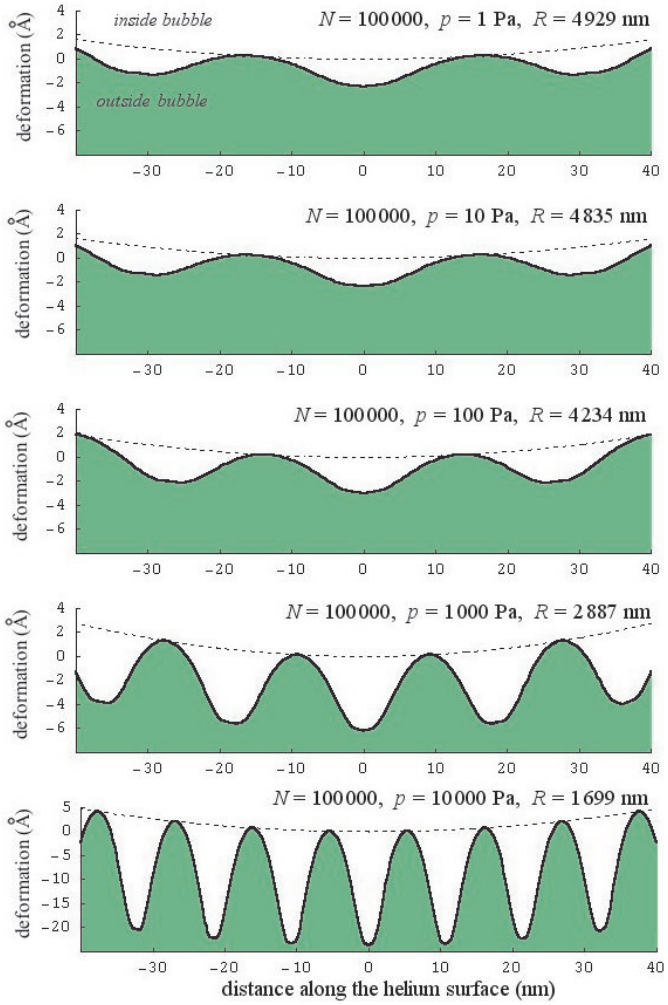

Fig. 2. For a bubble with $N = 10^5$ electrons the shape of the dimpled surface is shown at different pressures. Electrons are present on the surface, separated from each other by the lattice parameter d. Underneath each electron there is an individual dimple, induced by the electron-ripplon interaction. As the pressure is increased, the bubble radius decreases, and the electron-ripplon interaction becomes stronger, resulting in a stronger dimpling effect.

The electrons are separated by the interelectron distance $d = \sqrt{4\pi R_b^2/N}$. As the pressure increases, the radius of the bubble decreases. Since the number of electrons is fixed the electric pressing field increases, making on its turn the electron-ripplon coupling larger. This results in deeper, narrower dimples. Note that while the deformation here can be several angstroms, for a flat surface on bulk helium the maximum deformation of a dimple is less than one angstrom [18]. Also for electrons on a thin helium film above a dielectric substrate, the dimple depth can reach several angstroms [19].

4 The ripplopolaron Wigner lattice at finite temperature

The simple but intuitive approach of the previous section describes the system in the limit of temperature zero. To study the ripplopolaron Wigner lattice at finite temperature (and for any value of the electron-ripplon coupling), we use the variational path-integral approach [20]. This variational principle distinguishes itself from Rayleigh-Ritz variation in that it uses a trial action functional S_{trial} instead of a trial wave function.

The action functional of the system described by Hamiltonian (6), becomes, after elimination of the ripplon degrees of freedom,

$$S = -\frac{1}{\hbar}\int_0^{\hbar\beta} \mathrm{d}\tau \left\{\frac{m_e}{2}\dot{r}^2(\tau) + V_{lat}[r(\tau)]\right\} + \sum_{\mathbf{q}} |M_q|^2 \times \int_0^{\hbar\beta}\mathrm{d}\tau \int_0^{\hbar\beta}\mathrm{d}\sigma G_{\omega(q)}(\tau-\sigma)\mathrm{e}^{\mathrm{i}\mathbf{q}\cdot[\mathbf{r}(\tau)-\mathbf{r}(\sigma)]}, \quad (20)$$

with

$$G_\nu(\tau-\sigma) = \frac{\cosh[\nu(|\tau-\sigma| - \hbar\beta/2)]}{\sinh(\beta\hbar\nu/2)}. \quad (21)$$

In preparation of its customary use in the Jensen-Feynman inequality, the action functional (20) is written in imaginary time $t = \mathrm{i}\tau$ with $\beta = 1/(k_B T)$ where T is the temperature. Following an approach analogous to that of Fratini and Quémerais for a lattice of polarons in a semiconductor [15], and to that of Devreese *et al.* for N polarons in a quantum dot [21], we introduce a quadratic trial action of the form

$$S_{trial} = -\frac{1}{\hbar}\int_0^{\hbar\beta}\mathrm{d}\tau\left[\frac{m_e}{2}\dot{r}^2(\tau) + \frac{m_e\Omega^2}{2}r^2(\tau)\right] - \frac{Mw^2}{4\hbar}\int_0^{\hbar\beta}\mathrm{d}\tau\int_0^{\hbar\beta}\mathrm{d}\sigma G_w(\tau-\sigma)\mathbf{r}(\tau)\cdot\mathbf{r}(\sigma), \quad (22)$$

where M, w, and Ω are the variationally adjustable parameters. This trial action corresponds to the Lagrangian

$$\mathcal{L}_0 = \frac{m_e}{2}\dot{r}^2 + \frac{M}{2}\dot{R}^2 - \frac{\kappa}{2}r^2 - \frac{K}{2}(\mathbf{r}-\mathbf{R})^2, \quad (23)$$

from which the degrees of freedom associated with $\mathbf{R}$ have been integrated out. This Lagrangian can be interpreted as describing an electron with mass m_e at position $\mathbf{r}$, coupled through a spring with spring constant κ to its lattice site, and to which a fictitious mass M at position $\mathbf{R}$ has been attached with another spring, with spring constant K. The relation between the spring constants in (23) and the variational parameters w, Ω is given by

$$w = \sqrt{K/m_e}, \quad (24)$$

$$\Omega = \sqrt{(\kappa+K)/m_e}. \quad (25)$$

Based on the trial action S_{trial}, Feynman's variational method allows one to obtain an upper bound for the free energy F of the system (at temperature T) described by the action functional S by minimizing the following function:

$$F = F_0 - \frac{1}{\beta}\left\langle S - S_{trial}\right\rangle, \quad (26)$$

with respect to the variational parameters of the trial action. In this expression, F_0 is the free energy of the trial system characterized by the Lagrangian $\mathcal{L}_0$, $\beta = 1/(k_b T)$ is the inverse temperature, and the expectation value $\langle S - S_{trial} \rangle$ is to be taken with respect to the ground state of this trial system. The evaluation of expression (26) is straightforward though lengthy. We find

$$\begin{aligned} F = & \frac{2}{\beta} \ln \left[2 \sinh \left(\frac{\beta \hbar \Omega_1}{2} \right) \right] + \frac{2}{\beta} \ln \left[2 \sinh \left(\frac{\beta \hbar \Omega_2}{2} \right) \right] \\ & - \frac{2}{\beta} \ln \left[2 \sinh \left(\frac{\beta \hbar w}{2} \right) \right] - \frac{\hbar}{2} \sum_{i=1}^{2} a_i^2 \Omega_i \coth \left(\frac{\beta \hbar \Omega_i}{2} \right) \\ & - \frac{\sqrt{\pi} e^2}{D} \mathrm{e}^{-d^2/(2D)} \left[I_0 \left(\frac{d^2}{2D} \right) + I_1 \left(\frac{d^2}{2D} \right) \right] \\ & - \frac{1}{2\pi\hbar\beta} \int_{1/R_b}^{\infty} \mathrm{d}q q |M_q|^2 \int_0^{\hbar\beta/2} \mathrm{d}\tau \frac{\cosh[\omega(q)(\tau - \hbar\beta/2)]}{\sinh[\beta\hbar\omega(q)/2]} \\ & \times \exp \left[- \frac{\hbar q^2}{2m_e} \sum_{j=1}^{2} a_j^2 \frac{\cosh(\hbar\Omega_j \beta/2) - \cosh[\hbar\Omega_j(\tau - \beta/2)]}{\Omega_j \sinh(\hbar\Omega_j \beta/2)} \right] . \quad (27) \end{aligned}$$

In this expression, I_0 and I_1 are Bessel functions of imaginary argument, and

$$D = \frac{\hbar}{m_e} \sum_{j=1}^{2} \frac{a_j^2}{\Omega_j} \coth \left(\hbar \Omega_j \beta / 2 \right) , \quad (28)$$

$$a_1 = \sqrt{\frac{\Omega_1^2 - w^2}{\Omega_1^2 - \Omega_2^2}}; a_2 = \sqrt{\frac{w^2 - \Omega_2^2}{\Omega_1^2 - \Omega_2^2}}. \quad (29)$$

Finally, Ω_1 and Ω_2 are the eigenfrequencies of the trial system, given by

$$\Omega_{1,2}^2 = \frac{1}{2} \left[\Omega^2 + w^2 \pm \sqrt{\left(\Omega^2 - w^2 \right)^2 + 4K/(M m_e)} \right] . \quad (30)$$

Optimal values of the variational parameters are determined by the numerical minimization of the variational functional F as given by expression (27). As the reader may notice, the result of the variational path-integral method is slightly less intuitive than that of the strong-coupling approach of the previous section, nevertheless it is much more general and will allow us to introduce temperature to examine the melting of the Wigner lattice of ripplopolarons in the next section.

5 Melting of the ripplopolaron Wigner lattice

The Lindemann melting criterion [16] states in general that a crystal lattice of objects (be it atoms, molecules, electrons, or ripplopolarons) will melt when the average motion of the objects around their lattice site is larger than a critical fraction δ_0 of the lattice parameter d. It would be a strenuous task to calculate from first principles the exact value of the critical fraction δ_0, but for the particular case of electrons on a helium surface, we can make use of an experimental determination. Grimes and Adams [22] found that the Wigner lattice melts when $\Gamma = 137 \pm 15$, where Γ is the ratio of potential energy to the kinetic energy per electron. In their experiment, the electron density varied from 10^8 cm^{-2} to 3×10^8 cm^{-2} while the melting temperature T_c varied from 0.23 K to 0.66 K. At temperature T the average kinetic energy in a lattice potential V_{lat} is

$$E_{kin} = \frac{\hbar\omega_{lat}}{2} \coth \left(\frac{\hbar\omega_{lat}}{2k_B T} \right) , \quad (31)$$

and the average distance that an electron moves out of the lattice site is determined by

$$\left\langle \mathbf{r}^2 \right\rangle = \frac{\hbar}{m_e \omega_{lat}} \coth \left(\frac{\hbar\omega_{lat}}{2k_B T} \right) = \frac{2E_{kin}}{m_e \omega_{lat}^2}. \quad (32)$$

From this we find that for the melting transition in Grimes and Adams' experiment [22], the critical fraction equals $\delta_0 \approx 0.13$. This estimate is in agreement with previous (empirical) estimates yielding $\delta_0 \approx 0.1$ [23], and we shall use it in the rest of this paper.

The unmodified Lindemann criterion as stated above cannot be applied to an infinite layer of electrons on helium at non-zero temperature, because (when a thermal occupation of the ripplon modes is assumed) a straightforward calculation of the average distance that an electron moves out of its lattice site yields a divergent result. This divergence is closely related to Hohenberg's theorem forbidding Bose-Einstein condensation in 2D. Therefore, many authors rely on a modified Lindemann criterion [24] that considers the average distance between two nearest neighbors instead of the average distance of a lattice resident from its lattice site. However, for the current geometry this modification is unnecessary: the multielectron bubble is a finite and confined system, for which considerations based on Hohenberg's theorem do not apply. Hence, we shall use the unmodified Lindemann criterion to study the melting of the ripplopolaron lattice. In practice, we see that the above-mentioned divergence is not present because there is a natural cut-off wavelength for the ripplons: the lowest ripplon mode on a sphere corresponds to an $\ell = 1$ spherical harmonic, to which a characteristic wavelength of the order of $1/R_b$ can be associated. We have checked that the results do not depend on the precise value of the cut-off wavelength λ/R_b with λ on the order of 1.

Within the approach of Fratini and Quémerais [15], the Wigner lattice of (ripplo)polarons melts when at least one of the two following Lindemann criteria are met:

$$\delta_r = \frac{\sqrt{\langle \mathbf{R}_{cms}^2 \rangle}}{d} > \delta_0, \quad (33)$$

$$\delta_\rho = \frac{\sqrt{\langle \rho^2 \rangle}}{d} > \delta_0. \quad (34)$$

where ρ and $\mathbf{R}_{cms}$ are, respectively, the relative coordinate and the center of mass coordinate of the model system (23): if $\mathbf{r}$ is the electron coordinate and $\mathbf{R}$ is

the position coordinate of the fictitious ripplon mass M, this is

$$\mathbf{R}_{cms} = \frac{m_e\mathbf{r} + M\mathbf{R}}{m_e + M}; \rho = \mathbf{r} - \mathbf{R}. \tag{35}$$

The appearance of two Lindemann criteria takes into account the composite nature of (ripplo)polarons. As follows from the physical sense of the coordinates ρ and $\mathbf{R}_{cms}$, the first criterion (33) is related to the melting of the ripplopolaron Wigner lattice towards a ripplopolaron liquid, where the ripplopolarons move as a whole, the electron together with its dimple. The second criterion (34) is related to the dissociation of ripplopolarons: the electrons shed their dimple.

The path-integral variational formalism outlined in the previous section allows us to calculate the expectation values $\langle \mathbf{R}_{cms}^2 \rangle$ and $\langle \rho^2 \rangle$ with respect to the ground state of the variationally optimal model system. We find

$$\begin{aligned}\langle \mathbf{R}_{cms}^2 \rangle = & \frac{\hbar w^4}{m_e \left[w^2(\Omega_1^2 + \Omega_2^2) - \Omega_1^2\Omega_2^2\right](\Omega_1^2 - \Omega_2^2)} \\ & \times \left[\Omega_2^4(\Omega_1^2 - w^2)\coth(\hbar\Omega_1\beta/2)/\Omega_1 \right. \\ & \left. + \Omega_1^4(w^2 - \Omega_2^2)\coth(\hbar\Omega_2\beta/2)/\Omega_2\right], \end{aligned} \tag{36}$$

$$\begin{aligned}\langle \rho^2 \rangle = & \frac{\hbar}{m_e(\Omega_1^2 - \Omega_2^2)(\Omega_1^2 - w^2)(w^2 - \Omega_2^2)} \\ & \times \left[\Omega_1^3(w^2 - \Omega_2^2)\coth(\hbar\Omega_1\beta/2) \right. \\ & \left. + \Omega_2^3(\Omega_1^2 - w^2)\coth(\hbar\Omega_2\beta/2)\right]. \end{aligned} \tag{37}$$

The procedure to find whether the Lindemann criteria are fulfilled is then as follows: first the optimal values of the variational parameters are obtained by minimization of the free energy (27), and then these optimal values are substituted in (36, 37). Numerical calculation shows that for ripplopolarons in an MEB the inequality $\Omega_1 \gg w$ is fulfilled ($w/\Omega_1 \approx 10^{-3}$ to 10^{-2}) so that the strong-coupling regime is realized, in agreement with the results of Section 2. Owing to this inequality, we find from equations (36, 37) that

$$\langle \mathbf{R}_{cms}^2 \rangle \ll \langle \rho^2 \rangle. \tag{38}$$

So, the destruction of the ripplopolaron Wigner lattice in an MEB occurs through the dissociation of ripplopolarons, since the second criterion (34) will be fulfilled before the first (33). The results for the melting of the ripplopolaron Wigner lattice are summarized in the phase diagram shown in Figure 3. For every value of N, pressure p and temperature T in an experimentally accessible range, this figure shows whether the ripplopolaron Wigner lattice is present (points above the surface) or molten (points below the surface). Below a critical pressure (on the order of 10^4 Pa) the ripplopolaron solid will melt into an electron liquid. This critical pressure is nearly independent of the number of electrons (except for the smallest bubbles) and is weakly temperature dependent, up to the helium critical temperature 5.2 K. This can be understood since the typical lattice potential well in which the ripplopolaron resides has frequencies of the order of THz or larger, which correspond to ~ 10 K.

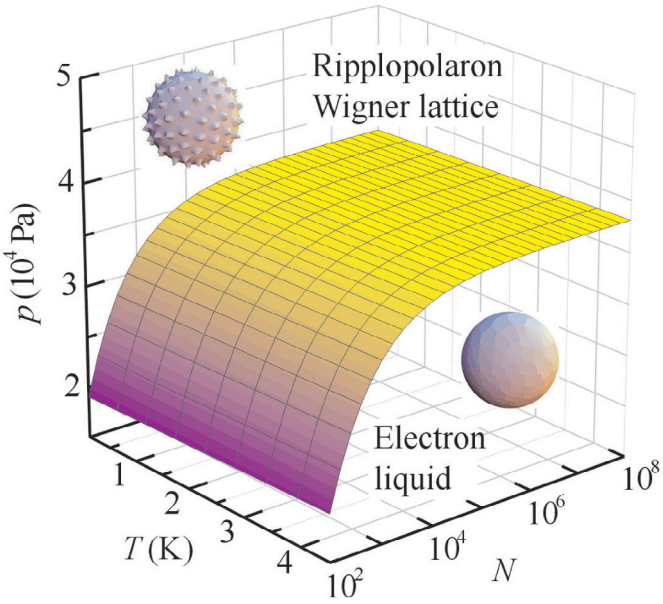

Fig. 3. The phase diagram for the spherical 2D layer of electrons in the MEB. Above a critical pressure, a ripplopolaron solid (a Wigner lattice of electrons with dimples in the helium surface underneath them) is formed. Below the critical pressure, the ripplopolaron solid melts into an electron liquid through dissociation of ripplopolarons.

6 Discussion

In the previous section we have established that the ripplopolaron Wigner lattice will not melt into a liquid of ripplopolarons, but rather melt through dissociation of the composite quasiparticle that is the ripplopolaron. The absence of a ripplopolaron liquid phase can be understood intuitively from the fact that the ripplon frequencies (typically GHz) are several orders of magnitude smaller than the electron frequencies in the lattice potential (typically THz). In order to create a liquid of ripplopolarons, the ripplopolarons have to move with an average velocity large enough to keep the ripplopolaron lattice molten. This motion has to be of the entire object, namely the electron and its dimple. But, at the velocities required to keep the ripplopolaron liquid from freezing into a lattice, the dimples cannot follow the electrons. Thus, ripplopolarons only exist in a crystallized state.

The present treatment does not allow us to derive the structure of this lattice – the mean-field approximation made for the lattice potential prohibits this. The problem of the exact lattice structure is complicated by the topology of the surface [25]: unlike for a flat surface, it is impossible to tile a sphere with a triangular lattice. Frustration of the lattice in the form of point defects is unavoidable, providing nucleation points for melting the lattice. The problem of placing classical point charges on a sphere was first considered by Thomson [26] and was recently reconsidered for localized electrons in multielectron bubbles [27].

The present treatment does allow us to also study the electron Wigner lattice, by putting $e|\mathbf{E}| = 0$ in the above results, thus switching the electron-ripplon coupling off. A Wigner lattice of electrons is to be distinguished from a Wigner lattice of ripplopolarons. The lattice of ripplopolarons on the one hand melts through dissociation of the ripplopolarons, and this melting line is almost temperature independent. The lattice of electrons on the other hand melts through either classical thermal motion (when the temperature reaches a melting temperature of about 0.5 K), or through quantum melting when the density of electrons is large enough so that the extent of the zero-point motion becomes comparable to the lattice parameter. In the Wigner lattice of the ripplopolarons, the particles are localized by the self-induced polaronic trapping potential (the dimple) due to the electron-ripplon interaction. In the Wigner lattice of electrons, the electrons are localized through the Coulomb interaction between the electrons. Finally, the region in phase space where the ripplopolaron Wigner lattice resides is different from the region where the electron Wigner lattice is found. This is illustrated in Figure 4, where the phase diagram drawn in Figure 3 is extended to huge bubbles (approaching the flat surface geometry). In the corner of largest N ($N > 10^9$, $R_b \gtrsim 1$ mm, $n_s \lesssim 10^9$–10^{10} cm^{-2}) and lowest pressure ($p < 0.1$ Pa), we find that an electron Wigner lattice (without individual dimples) can still be formed below $T = 0.4$ K. Thus, the electron Wigner lattice is recovered and the melting temperature derived from our treatment is in agreement with the experimentally observed temperature [22]. Our calculations show that, as the bubble is compressed, the electron Wigner lattice will quantum melt because of the increased density of electrons. The region of phase space where the electron Wigner lattice is present is separated from the region where the ripplopolaron Wigner lattice is present by a region where the predicted phase is an electron liquid. The ripplopolaron liquid phase, as mentioned before, does not exist. Since, as mentioned in the previous paragraph, our method does not allow us to study the crystal structure, we cannot, in the electron Wigner lattice phase, distinguish between the crystalline and the hexatic phase [28].

The new phase that we predict, the ripplopolaron Wigner lattice, will not be present for electrons on a flat helium surface. At the values of the pressing field necessary to obtain a strong enough electron-ripplon coupling, the flat helium surface is no longer stable against long-wavelength deformations [9]. Multielectron bubbles, with their different ripplon dispersion and the presence of stabilizing factors such as the energy barrier against fissioning [10], allow for much larger electric fields pressing the electrons against the helium surface. The regime of N, p, T parameters suitable for the creation of a ripplopolaron Wigner lattice lies within the regime that would be achievable in recently proposed experiments aimed at stabilizing multielectron bubbles [29]. The ripplopolaron Wigner lattice and its melting transition might be detected by spectroscopic techniques [22,30] probing for example the transverse phonon modes of the lattice [31].

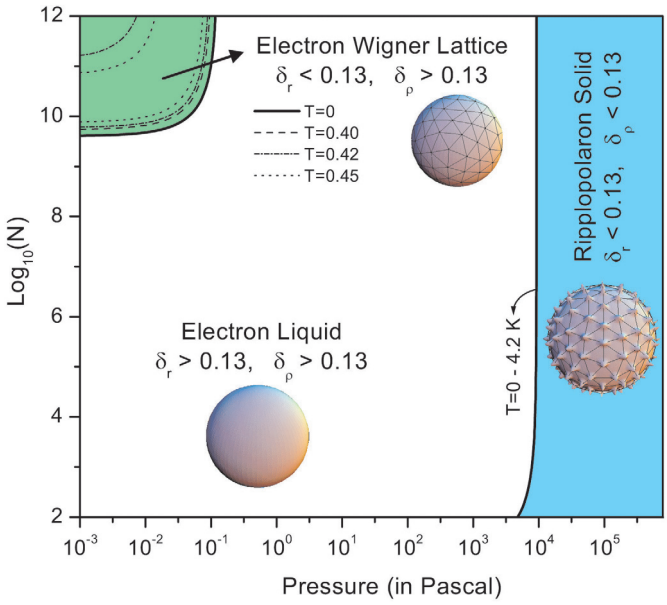

Fig. 4. The phase diagram, shown in Figure 3 is extended to reveal the relation of the ripplopolaron Wigner lattice to the Wigner lattice of electrons. These are distinct, not only in melting properties (the ripplopolaron Wigner lattice melts through dissociation of ripplopolarons), but also in their location on the phase diagram. The region for the Wigner lattice of electrons without dimples –in agreement with the observation of Grimes and Adams [22] – starts at large N and is quantum molten by pressurizing the bubble.

7 Conclusions

In this paper, we investigate the properties of ripplopolarons in a multielectron bubble in helium using path-integral methods similar to those developed for a lattice of polarons [15]. Expressions are derived for the free energy and the dimple shape of ripplopolarons in a Wigner lattice in a multielectron bubble, as a function of temperature, externally applied pressure and number of electrons in the bubble. We find that, owing to the difference in the ripplon and longitudinal plasmon frequencies [17], the ripplopolarons exist only in a Wigner crystallized state. This state differs from the Wigner lattice of electrons, in that the electrons in the ripplopolaron Wigner lattice are localized by the electron-ripplon interaction rather than the Coulomb repulsion, and in that the melting occurs through the dissociation of the ripplopolarons. As electron-ripplon interaction is weakened (for example by reducing the externally applied pressure on the multielectron bubble) the electrons can shed their localized dimple and the ripplopolaron Wigner state is destroyed. The melting transition is shown to occur in a region of phase space that is accessible to recently proposed experiments for stabilizing multielectron bubbles.

The authors would like to acknowledge V.M. Fomin for helpful discussions and intensive interactions. Discussions with J. Huang are gratefully acknowledged. J.T. is supported financially by the FWO-Flanders. This research has been supported

by the Department of Energy, Grant DE-FG02-ER45978, and by the GOA BOF UA 2000, IUAP, the FWO-V projects Nos. G.0435.03, G.0274.01, G.0306.00.

Appendix A: Electron-ripplon interaction in MEBs

A.1 Ripplon dispersion on a sphere

The modes of oscillation of the bubble surface will be called 'ripplons' in analogy with the surface oscillations on a flat helium surface. In general, the deformed bubble surface can be described by a function $R(\Omega)$ which gives the distance, from the center of the bubble, of the bubble surface in the direction determined by the spherical angles $\Omega = \{\theta, \phi\}$. The deformation $u(\Omega)$ from spherical symmetry can be expanded in spherical harmonics $Y_{\ell m}(\Omega)$:

$$R(\Omega) = R_b + u(\Omega) = R_b + \sum_{\ell,m} Q_{\ell,m} Y_{\ell,m}(\Omega). \tag{39}$$

In this expression, R_b is the angle-averaged radius, and $Q_{\ell m}$ is the amplitude of the deformational mode corresponding to the spherical harmonic $Y_{\ell,m}$. In the summation, we abbreviate $\sum_{\ell,m} = \sum_{\ell=1}^{\infty} \sum_{m=-\ell}^{\ell}$. The equilibrium bubble radius is found by balancing the surface tension and pressure terms with the Coulomb repulsion: R_b satisfies

$$2\sigma R_b + pR_b^2 = \frac{e^2}{4\pi\varepsilon R_b^2}, \tag{40}$$

with $\sigma \approx 3.6 \times 10^{-4}$ J/m^2 the surface tension of helium, $\varepsilon = 1.0572$ the dielectric constant of helium, p the difference in pressure outside and inside the bubble, e the electron charge and N the number of electrons in the bubble. Expanding the energy of the bubble up to second order in $Q_{\ell m}$ allows to derive the frequency of oscillation of a particular mode of deformation [8]:

$$\omega(\ell) = \sqrt{\frac{\ell+1}{\rho R_b^3}\left[\sigma(\ell^2+\ell+1) + pR_b - \frac{N^2e^2}{4\pi\varepsilon R_b^3}\frac{\ell^2-\varepsilon(\ell+1)}{\ell+\varepsilon(\ell+1)}\right]}, \tag{41}$$

where $\rho \approx 145$ kg/m^3 the mass density of helium. Thus, for small amplitude deformations of the bubble, we find that the shape of the bubble oscillates with frequencies given by (41). Taking the bare ripplon frequency (without the effect of the interaction with electrons) and putting $R_b \to \infty$ (with $\ell/R_b = q$ a constant) we find

$$\omega^{bare}_{R_b\to\infty}(q) = \sqrt{\frac{\sigma}{\rho}q^3 + \frac{pR_b}{\rho}q}. \tag{42}$$

This dispersion relation corresponds to the ripplon dispersion on the flat surface, with the difference that there is in our dispersion relation no gravitational term, but a term related to the pressure on the bubble.

A.2 Electron ripplon interaction in the MEB

The interaction energy between the ripplons and the electrons in the multielectron bubble can be derived from the following considerations: (i) the distance between the layer of electrons and the helium surface is fixed (the electrons find themselves confined to an effectively 2D surface anchored to the helium surface [5]) and (ii) the electrons are subjected to a force field, arising from the electric field of the other electrons. For a spherical bubble, this electric field lies along the radial direction and equals

$$\mathbf{E} = -\frac{Ne}{2R_b^2}\mathbf{e_r}. \tag{43}$$

A bubble shape oscillation will displace the layer of electrons anchored to the surface. The interaction energy which arises from this, equals the displacement of the electrons times the force $e\mathbf{E}$ acting on them. Thus, we get for the interaction Hamiltonian

$$\hat{H}_{int} = \sum_j e|\mathbf{E}| \times u(\hat{\Omega}_j). \tag{44}$$

Here $u(\Omega)$ is the radial displacement of the surface in the direction given by the spherical angle Ω; and $\hat{\Omega}_j$ is the (angular) position operator for electron j. The displacement can be rewritten using (39) and we find

$$\hat{H}_{int} = \sum_j e|\mathbf{E}| \sum_{\ell,m} \hat{Q}_{\ell m} Y_{\ell m}(\hat{\Omega}_j). \tag{45}$$

Using the relation

$$\hat{Q}_{\ell,m} = (-1)^{(m-|m|)/2}\sqrt{\tfrac{\hbar(\ell+1)}{2\rho R_b^3\omega_\ell}}(\hat{a}_{\ell,m} + \hat{a}^+_{\ell,-m}), \tag{46}$$

the interaction Hamiltonian can be written in the suggestive form

$$\hat{H}_{int} = \sum_{\ell,m}\sum_j M_{\ell,m} Y_{\ell,m}(\hat{\Omega}_j)(\hat{a}_{\ell,m} + \hat{a}^+_{\ell,-m}), \tag{47}$$

with the electron-ripplon coupling amplitude for a MEB given by

$$M_{\ell,m} = (-1)^{(m-|m|)/2}\frac{Ne^2}{2R_b^2}\sqrt{\frac{\hbar(\ell+1)}{2\rho R_b^3\omega_\ell}}. \tag{48}$$

A.3 Locally flat approximation

Substituting $M_{\ell,m}$ into (47), we get

$$\hat{H}_{int} = \sum_{\ell,m}\sum_j \frac{Ne^2}{2R_b^2}\sqrt{\frac{\hbar(\ell+1)}{2\rho R_b^3\omega_\ell}} \times \left[(-1)^{(m-|m|)/2}\frac{Y_{\ell,m}(\hat{\Omega}_j)}{R_b}\right](\hat{a}_{\ell,m} + \hat{a}^+_{\ell,-m}). \tag{49}$$

In this expression, we consider the limit of a bubble so large that the surface becomes flat on all length scales of interest. Hence we let $R_b \to \infty$ but keep $\ell/R_b = q$ a constant. This means we have to let $\ell \to \infty$ as well. In this limit,

$$\lim_{\ell\to\infty} Y_{\ell,0}(\theta) = \frac{\mathrm{i}^\ell}{\pi\sqrt{\sin\theta}} \sin[(\ell+1/2)\theta + \pi/4], \qquad (50)$$

and $Y_{\ell,0}(\theta)$ varies locally as a plane wave with wave vector $q = \ell/R_b$. The wave function $Y_{\ell,m}(\hat{\Omega}_j)/R_b$ is furthermore normalised with respect to integration over the surface (with total area $4\pi R_b^2$). Thus, we get in the locally flat approximation

$$\hat{H}_{int} = \sum_{\mathbf{q}} \sum_j \frac{Ne^2}{2R_b^2} \sqrt{\frac{\hbar q}{2\rho\omega(q)}} \mathrm{e}^{\mathrm{i}\mathbf{q}\cdot\hat{\mathbf{r}}_j} (\hat{a}_{\mathbf{q}} + \hat{a}^+_{-\mathbf{q}}), \qquad (51)$$

or

$$\hat{H}_{int} = \sum_{\mathbf{q}} \sum_j M_q \mathrm{e}^{\mathrm{i}\mathbf{q}\cdot\hat{\mathbf{r}}_j} (\hat{a}_{\mathbf{q}} + \hat{a}^+_{-\mathbf{q}}),$$

$$M_q = e|\mathbf{E}| \sqrt{\frac{\hbar q}{2\rho\omega(q)}}. \qquad (52)$$

This corresponds in the limit of large bubbles to the interaction Hamiltonian expected for a flat surface.

References

1. *Two-dimensional electron systems on helium and other cryogenic substrates*, edited by E.Y. Andrei (Kluwer Acad. Publ., Dordrecht, The Netherlands, 1997)
2. V.B. Shikin, Zh. Eksp. Teor. Fiz. **58**, 1140 (1970) [Sov. Phys. JETP **31**, 936 (1970)]
3. A.P. Volodin, M.S. Khaikin, V.S. Edelman, Pis'ma Zh. Eksp. Teor. Fiz. **26**, 707 (1977) [JETP Lett. **26**, 543 (1977)]; U. Albrecht, P. Leiderer, Europhys. Lett. **3**, 705 (1987)
4. V.B. Shikin, JETP Lett. **27**, 39 (1978); M.M. Salomaa, G.A. Williams, Phys. Rev. Lett. **47**, 1730 (1981)
5. M.M. Salomaa, G.A. Williams, Phys. Rev. Lett. **47**, 1730 (1981)
6. V.V. Rotkin, R.A. Suris, Sov. Solid State Physics **36**, 1899 (1994)
7. R.D. Averitt, D. Sarkar, N.J. Halas, Phys. Rev. Lett. **78**, 4217 (1997); E. Prodan, P. Nordlander, Chem. Phys. Lett. **352**, 140 (2002)
8. J. Tempere, I.F. Silvera, J.T. Devreese, Phys. Rev. Lett. **87**, 275301 (2001)
9. L.P. Gor'kov, D.M. Chernikova, Pis'ma Zh. Eksp. Teor. Fiz. **18**, 119 (1973) [JETP Lett. **18**, 68 (1973)]
10. J. Tempere, I.F. Silvera, J.T. Devreese, Phys. Rev. B **67**, 035402 (2003)
11. V.B. Shikin, Yu.P. Monarkha, Zh. Eksp. Teor. Fiz. **65**, 751 (1973) [Sov. Phys. JETP **38**, 373 (1973)]
12. H. Fröhlich, Advances in Physics **3**, 325 (1954)
13. S.A. Jackson, P.M. Platzman, Phys. Rev. B **24**, 499 (1981); Phys. Rev. B **25**, 4886 (1982)
14. S.A. Jackson, F.M. Peeters, Phys. Rev. B **30**, 4196 (1984)
15. S. Fratini, P. Quémerais, Eur. Phys. J. B **14**, 99 (2000); Eur. Phys. J. B **29**, 41 (2002)
16. F. Lindemann, Z. Phys. **11**, 609 (1910); C.M. Care, N.H. March, Adv. Phys. **24**, 101 (1975)
17. S.N. Klimin, V.M. Fomin, J. Tempere, I.F. Silvera, J.T. Devreese, accepted for publication in Solid State Comm.
18. H. Ikezi, R.W. Gianetta, P.M. Platzman, Phys. Rev. B **25**, 4488 (1982)
19. G.E. Marques, N. Studart, Phys. Rev. B **39**, 4133 (1989)
20. R.P. Feynman, Phys. Rev. **97**, 660 (1955); R.P. Feynman, A.R. Hibbs, *Quantum Mechanics and Path Integrals* (Mc Graw-Hill, New York, 1965)
21. J.T. Devreese, S.N. Klimin, V.M. Fomin, F. Brosens, Solid State Commun. **114**, 305 (2000)
22. C.C. Grimes, G. Adams, Phys. Rev. Lett. **42**, 795 (1979)
23. V.M. Bedanov, F.M. Peeters, Phys. Rev. B **49**, 2667 (1994)
24. V.M. Bedanov, G.V. Gadiyak, Y.E. Lozovik, Phys. Lett. A **109**, 289 (1985)
25. A. Pérez-Garrido, M.J.W. Dodgson, M.A. Moore, Phys. Rev. B **56**, 3640 (1997)
26. J.J. Thomson, Philos. Mag. **7**, 237 (1904)
27. P. Lenz, D.R. Nelson, Phys. Rev. Lett. **87**, 125703 (2001)
28. D.R. Nelson, B.I. Halperin, Phys. Rev. B **19**, 2457 (1979)
29. I.F. Silvera, Bull. Am. Phys. Soc. **46**, 1016 (2001)
30. D.S. Fisher, B.I. Halperin, P.M. Platzman, Phys. Rev. Lett. **42**, 798 (1979)
31. G. Deville, A. Valdes, E.Y. Andrei, F.I.B. Williams, Phys. Rev. Lett. **53**, 588 (1984)